THE ASTROPHYSICAL JOURNAL, 513:983–989, 1999 March 10
© 1999. The American Astronomical Society. All rights reserved. Printed in U.S.A.

A STUDY OF MICROWAVE-SELECTED CORONAL TRANSIENT BRIGHTENINGS

A. NINDOS, M. R. KUNDU, AND S. M. WHITE
Astronomy Department, University of Maryland, College Park, MD 20742
Received 1998 October 2; accepted 1998 October 13

ABSTRACT

We present the results of a search for radio-selected transient brightenings (TBs) in the solar atmosphere as a complement to the more common X-ray–selected surveys. The Sun was generally quiet during the observations, making these data sensitive to weak TBs both in and outside active regions. Five small impulsive events were identified in a set of VLA observations at 4.5, 1.5, and 0.33 GHz and compared with soft X-ray images from *Yohkoh* and EUV images from *SOHO*/EIT. Four of the events were located at the edges of an active region, but one was located 100″ away in a quiet region of the atmosphere. Possible emission mechanisms for these brightenings are investigated. The time profiles of the radio TBs show impulsive peaks, while the corresponding soft X-ray profiles are gradual. The impulsive radio peaks were up to 35% polarized. Our data favor an interpretation in terms of gyrosynchrotron radiation from mildly relativistic electrons. A small number of nonthermal electrons with spectral index 3 can explain the observed properties of the TBs. Thus, nonthermal TBs can be found away from active regions. Two of the microwave TBs also show evidence for type III radio emission at 327 MHz.

Subject headings: Sun: activity — Sun: corona — Sun: radio radiation — Sun: X-rays, gamma rays

1. INTRODUCTION

Over the past years the soft X-ray imaging telescope (SXT) on board the *Yohkoh* satellite (Tsuneta et al. 1991) has revealed that the X-ray corona is far more dynamic than had previously been realized. The high spatial and temporal resolution of the SXT allowed the detection of small flarelike brightenings in active regions, which are called "active region transient brightenings" or just transient brightenings (TBs). X-ray TBs last 5–20 minutes and show great variety in X-ray morphology (Shimizu et al. 1994; Shimizu 1994). They appear mostly in the form of multiple or single loops, although some brightenings are pointlike. Their frequency of occurrence has a strong correlation with the total soft X-ray flux of the active region (Shimizu et al. 1992). The energy involved in the individual TBs is estimated to range from 10^{25} to 10^{29} ergs.

An important question is whether these events can be regarded as microflares or miniflares in the sense that they display evidence for acceleration of nonthermal electrons, or whether they just heat the coronal plasma with no associated nonthermal emission. Hard X-ray observations of TBs are not easily available because of the lack of the required sensitivity of the current hard X-ray telescopes. However, radio observations provide an alternative method to search for nonthermal effects because they are generally more sensitive to the presence of nonthermal electrons. Gopalswamy et al. (1994, 1997) used the VLA[1] at 2, 3.7, and 6 cm and detected TBs associated with soft X-ray brightenings near the penumbra of a sunspot. The radio sources were highly polarized and were inferred to be nonthermal. White et al. (1995) studied X-ray–selected events in an active region using simultaneous observations from the Nobeyama Radioheliograph and found similar time profiles in X-rays and radio, suggesting plasma heating rather than particle acceleration. Gary, Hartl, & Shimizu (1997) examined the total power Owens Valley Radio Observatory (OVRO) data in the range of 1–18 GHz during times when SXT detected several bright TBs. They found that some events showed nonthermal microwave spectra. Because of limitations of the OVRO solar array, imaging of the transient brightenings was not possible, thus the locations of the radio sources with respect to the soft X-ray TBs could not be determined. Krucker et al. (1997) studied a quiet region using deep-integration SXT images together with simultaneous VLA observations. They detected four extremely weak soft X-ray TBs above the magnetic network that were associated with flarelike radio emission.

Most studies of TBs have used soft X-ray data to select the brightenings and then investigated the properties of the X-ray sample at other wavelengths. In this paper, we adopt the opposite approach and investigate the properties of radio-selected TBs; we take 3 days of VLA observations and search for transient events. We then investigate the properties of these events at other wavelengths, where available. In principle, the radio-selected events may be quite different from soft X-ray–selected events: the latter are all due to the presence of dense heated plasma that produces free-free emission at radio wavelengths, but radio emission can be produced by nonthermal electrons or thermal emission in strong magnetic fields as well, and events detected via such emission may well be a different type of energy release.

The Sun was quiet during our observations. The absence of a strong active region made these data ideal for studying weak events inside and outside active regions rather than strong active region TBs such as those presented by Gary et al. (1997). Additional information was provided by soft X-ray images from *Yohkoh* SXT and from *SOHO* EIT. An advantage of our study was the availability of high spatial resolution images in both radio and in soft X-rays, which could be used to check whether or not weak phenomena at different wavelengths are truly associated.

2. OBSERVATIONS AND DATA REDUCTION

The VLA observations were carried out on 1997 June 27, 29, and 30. The C configuration was used to image the Sun at 4.53 GHz (C band), 1.46 GHz (L band), and 0.33 GHz (P

[1] The Very Large Array is a facility of the National Radio Astronomy Observatory, which is operated by Associated Universities, Inc., under cooperative agreement with the National Science Foundation.

TABLE 1

VLA OBSERVATIONS

Date (1997)	Start (UT)	End (UT)	Duration (hours)	Frequency (GHz)	Pointing	Beam Size (arcsec)
Jun 27.....	14:30	00:43	8:36	4.53	N15W42	5.1 × 4.7
	14:31	00:43	8:35	1.46	N02E09	19 × 13
	14:31	00:43	8:35	0.33	N02E09	90 × 57
Jun 29.....	13:52	23:35	8:11	4.53	N15W60	4.8 × 4.2
	13:53	23:36	8:10	1.46	N02E09	16 × 13
	13:53	23:36	8:10	0.33	N02E09	70 × 55
Jun 30.....	13:31	18:20	2:04	4.53	N15W60	6.1 × 4.4
	18:34	23:05	1:50	4.53	N15W60	4.6 × 4.6
	13:53	23:36	8:10	1.46	N02E09	16 × 13
	13:53	23:36	8:10	0.33	N02E09	70 × 55

band). On June 27 and 29, the array was split into two subarrays. One subarray was observed in LP bands, while the other was at C band. This yielded simultaneous coverage at three frequencies at the cost of reduced mapping ability. In the L-band and P-band the field of view covered the entire Sun, while in the C-band, it was limited to $\sim 10'$ and only the area around active region NOAA 8056 was imaged. A summary of the VLA observations is presented in Table 1.

For the 4.53 GHz data, the CLEAN algorithm was used to produce full-day maps while the 1.46 and 0.33 GHz data were reduced with the maximum entropy method. Because of instrumental problems, the June 27, 1.46 GHz left circularly polarized (L) data from an inner antenna were flagged. The quality of the resulting L map was not good, and the self-calibration technique did not improve the situation because the 1.46 GHz observations were obtained using one subarray only with the C configuration and the absence of an inner antenna created a large hole in the u-v coverage. The self-calibration of the 1.46 GHz L data using a CLEANed total intensity map as the input model did not improve the quality of the resulting map significantly. Thus, in our study of the June 27 1.46 GHz emission only the right circularly polarized (R) maps were used.

SXT images from *Yohkoh* were available for June 29 and June 30. Both full frame images and partial frame images were investigated. The partial frame images recorded active region NOAA 8056 with a time resolution of 64 s. The EIT on board *SOHO* also observed the Sun on June 27, 29, and 30. The field of view covered the entire Sun. However, the cadence of the EIT observations was not uniform; 30, 33, and 28 images were recorded at 195 Å during the time of the VLA observations on June 27, 29, and 30, respectively. In our study, the EIT images were used only in cases when *Yohkoh* images were not available.

The methodology of our study was to find radio TBs and then examine the corresponding *Yohkoh* (or EIT) images for soft X-ray counterparts of the radio events. For each VLA scan, the clean components of the full-day map were subtracted from the self-calibrated visibilities. This technique generally does not remove large-scale flux very well since it is not as well represented by the clean components. However, we expect on theoretical and observational grounds that transient features will be relatively compact, so we mapped the resulting visibilities using only the longer baselines. In cases where radio emission was more than 3 times the standard deviation σ of the dirty maps, the CLEAN algorithm was used to remove the sidelobes. Five TBs were detected using this procedure. Subsequently, snapshot maps with effective temporal resolution of 10 s were computed for these events. The dynamic range of the snapshot maps ranged from 7 to 10 allowing us to image fluxes as low as 1 mSFU (above the steady radio emission). Once the TBs were detected on the VLA maps, we computed soft X-ray difference images for the time intervals associated with the TBs by subtracting the active region emission using a prebrightening image.

3. OVERALL VIEW OF THE ACTIVE REGION

The active region near the center of the C-band field (see Fig. 1 for 4.5 GHz and soft X-ray images) was spotless and declining, and it was covered by a plage. According to Big Bear Solar Observatory (BBSO) Hα observations, a pore was present in its westernmost part. The L-band active region emission (see Fig. 2, *left-hand panel*) consisted of a compact source that covered the active region. The P-band maps showed that a weak bipolar noise storm was associated with the active region on June 27. On June 29 the active region had further declined such that the maximum intensity of the strongest 4.53 GHz component was 2.9 times lower than the corresponding intensity on the June 27 map. On June 30 the active region reached the limb and disappeared after 18:00 UT.

4. THE TRANSIENT BRIGHTENINGS

The observed properties (time range, frequency, duration of the impulsive peaks, noise of the snapshot maps, maximum flux, and maximum degree of circular polarization) of the TBs are presented in Table 2. The first event was only detected at L band (Fig. 2). No EIT frames were available close enough to the time interval when it occurred to be useful (*Yohkoh* images were not available for June 27). The GOES data showed a local peak at the time of maximum of the 1.46 GHz emission. No sign of that event appeared in the C-band observations (their rms noise was 0.0015 SFU) despite the fact that it was in the field of view and the spatial resolution was better than at L band.

The second TB on June 27 was observed at 4.53 GHz (see Fig. 3), with no L-band emission being detected. Again there were no EIT frames during the event. The event was not detected in the GOES data, suggesting that the excess soft X-ray emission was rather low.

In order to investigate whether the TBs affected the weak noise storm above the active region, we produced snapshot images of the 0.33 GHz emission using the technique

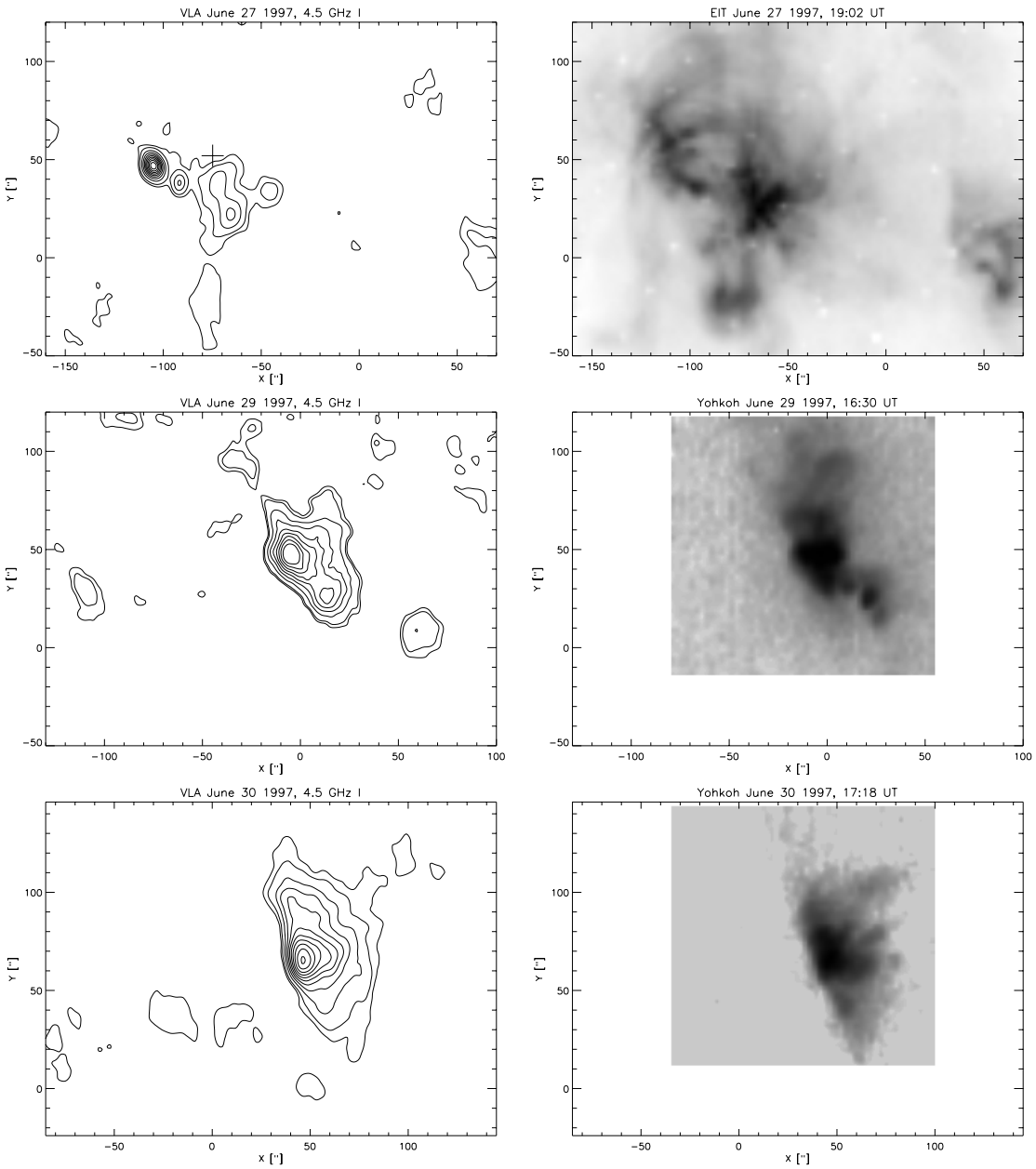

FIG. 1.—Contour plots of the VLA 4.53 GHz total intensity *I* full-day radio images (*left-hand column*) and gray-scale negative display of *Yohkoh* SXT or EIT images (*right-hand column*) for the active region NOAA 8056. Each row represents 1 day of observations (*top row*: 1997 June 27; *middle row*: 1997 June 29; *bottom row*: 1997 June 30). For June 27, a 195 Å EIT image obtained at 19:02 UT is shown, while for June 29 and June 30, partial *Yohkoh* images obtained with the thin aluminum filter at 16:30 UT and 17:18 UT, respectively, are presented. The contours are at multiples of 0.5, 1, 2, 3, 4, 5, 6, 7, 8, 9, and 10 of 60,000 K for the June 27 VLA map; 0.7, 1, 2, 3, 4, 5, 6, 7, 8, 9, and 10 of 21,000 K for the June 29 map; and 1, 2, 3, 4, 5, 6, 7, 8, 9, and 10 of 18,000 K for the June 30 map. The cross on the June 27 radio map indicates the centroid of the excess P-band emission at the time of the local 0.33 GHz maximum associated with the 18:13 UT TB (see § 4 for details). In this and subsequent solar images the axes labels indicate arcseconds from the VLA phase-tracking center. All solar images have been rotated so that solar north is up and solar east to the left.

TABLE 2

OBSERVED PROPERTIES OF RADIO TRANSIENT BRIGHTENINGS

Date (1997)	Frequency (GHz)	τ (s)	Detection Threshold (SFU)	Flux (SFU)	Polarization (%)
Jun 27 14:51–14:56.....	1.46	...	0.04	0.31	...
Jun 27 18:08–18:17.....	4.53	84	0.004	0.029	35 ± 10.7
Jun 29 16:30–16:36.....	4.53	45	0.002	0.017	33 ± 9.0
Jun 29 18:59–19:09.....	4.53	82	0.003	0.023	33 ± 8.6
Jun 30 17:19–17:26.....	4.53	40	0.002	0.019	27 ± 7.2

NOTE.—τ is the duration of impulsive peaks.

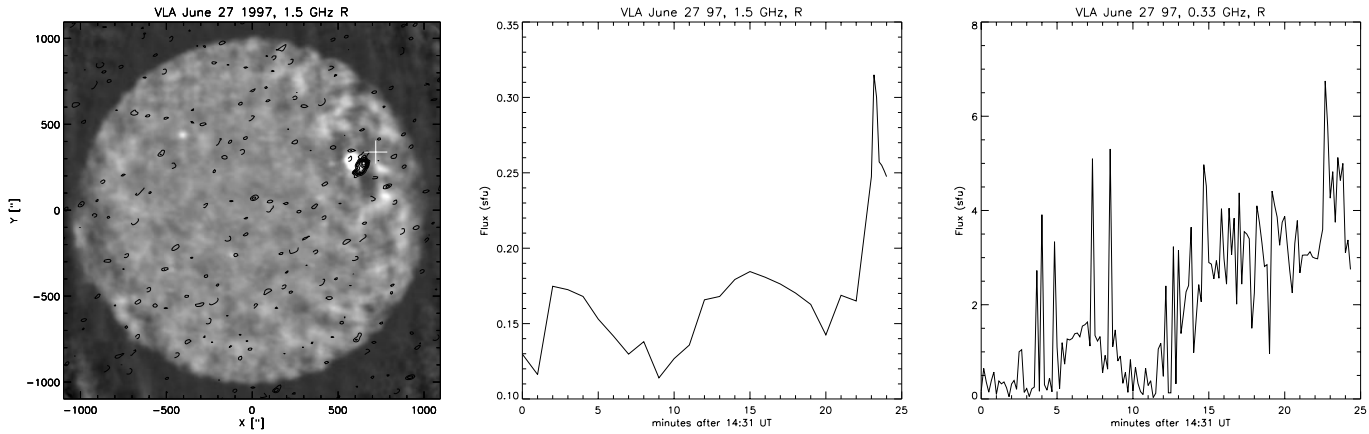

FIG. 2.—June 27 14:55 UT TB. Gray-scale representation of the full-day 1.46 GHz VLA *R* map overlain with contours of the snapshot 1.46 GHz image (see text for details on the method) of the TB at the time of its maximum (*left frame*). The contours are at multiples of −2, 2, 3, 4, 5, 6, 7, 8, 9, and 10 of 90,000 K. The cross indicates the centroid of the excess P-band emission at the time of the local 0.33 GHz maximum associated with the TB. Time profiles of the microwave emission from the TB at L band (*middle frame*) and P band (*right frame*).

described in § 2. Impulsive peaks of the excess P-band emission occurred at the rising phase of both events (see Fig. 2, *right-hand panel*, and Fig. 3, *bottom panel*), which are suggestive of type III–like events (Krüger 1979). However, there is an ambiguity about the spectral class of these events because they were too weak to be detected with frequency-agile instruments (e.g., the Nançay and the Potsdam instruments). The presence of the active region combined with the low resolution of the 0.33 GHz maps made it difficult to relate them to the TBs observed at 1.46 and 4.53 GHz. In order to remove this uncertainty, at least partially, we computed the centroids of the excess P-band emission at the times of the local 0.33 GHz maxima associated with the TBs (Figs. 2 and 3, *crosses*) and compared them with the centroid of the noise storm from the full-day map. The centroid of the 14:55 UT event was displaced 45″ closer to the centroid of the L-band TB. The displacement for the C-band event at 18:13 UT was 53″. These results, together with the temporal correlation, imply that indeed the observed P-band events were directly associated with the TBs observed at higher frequencies.

On July 29 two events were detected at 4.53 GHz. The first one (see Fig. 4, *top panels*) occurred at the edge of the active region. The event that was observed at 19:03 UT (see Fig. 4, *middle panels*) occurred 100″ away from the active region. According to the full-day map, a weak source was located there (the easternmost source on the contour plot of Fig. 1, *middle panels*). The *Yohkoh* observations ended at 16:50 UT, and that region was out of the field of view of the partial frame images. Full-disk EIT images were recorded at 18:56, 19:02, and 19:11 UT but did not show any signature of the source. Moreover, the GOES data did not show any excess X-ray emission during the same time interval. Michelson-Doppler Interferometer (MDI) images obtained at 16:00 UT and 20:48 UT did not show any photospheric manifestation of the source. No emission was detected at the location of the TB on June 30. This event was similar to the events described as network flares by Krucker et al. (1997), because it appeared far from the active region. On the other hand, it was different from those events because we did not detect any soft X-ray or photospheric/chromospheric counterparts. Here we should point out that it is well known (e.g., Wang, Zirin, & Ai 1991) that the lifetimes of network elements are usually longer than 50 hours. Computation of individual-scan maps at 4.53 GHz verified that the source in the full-day map, which was coincident with the TB, did not correspond to a steady source throughout the observing period.

One TB was observed on June 30, at 4.53 GHz only (see Fig. 4, *bottom panels*). The *Yohkoh* difference image showed a compact unresolved brightening at the location of the radio TB.

5. INTERPRETATION

In this section we investigate the possible emission mechanisms of the TBs using the available data. For numerical computations of the free-free emission, estimates of the local electron temperature, T_e, and emission measure, EM, are needed. Unfortunately, most of the *Yohkoh* images were obtained with the Al/Mg/Mn filter only. Only a limited number of frames on June 30 were observed with the thin aluminum filter. The Al/Mg/Mn-thin Al images observed closest to the time of the June 30 TB were obtained at 18:53 UT and 18:55 UT, respectively. Using that pair of images, we computed the T_e and EM at the location of the June 30 event. We found $T_e = 2.1 \times 10^6$ K and EM $= 3.8 \times 10^{27}$ cm^{-5}. The electron density N_e was calculated assuming that the line-of-sight depth of the June 30 TB was the same as its soft X-ray projected thickness. We found that $N_e = 2.2 \times 10^9$ cm^{-3}. Using the above values of N_e and T_e we found that the brightness temperature T_b predicted on the basis of thermal free-free emission from the observed soft X-ray material was 29,000 K. The brightness temperature of the full-day 4.53 GHz map at the same location was 30,000 K. In order to reproduce the observed brightness temperature associated with the June 30 TB (which was as high as 150,000 K), an increase of electron density by a factor of 2.2 was needed. This is not impossible since the electron density usually increases during the TB (see Gopalswamy et al. 1994).

On the other hand, a number of observable quantities of TBs could not be interpreted in terms of the free-free process. The microwave and soft X-ray time profiles of the TBs were not similar; the former showed impulsive peaks while the latter were more gradual. Moreover, the radio impulsive peaks showed polarizations 30%–35%. We

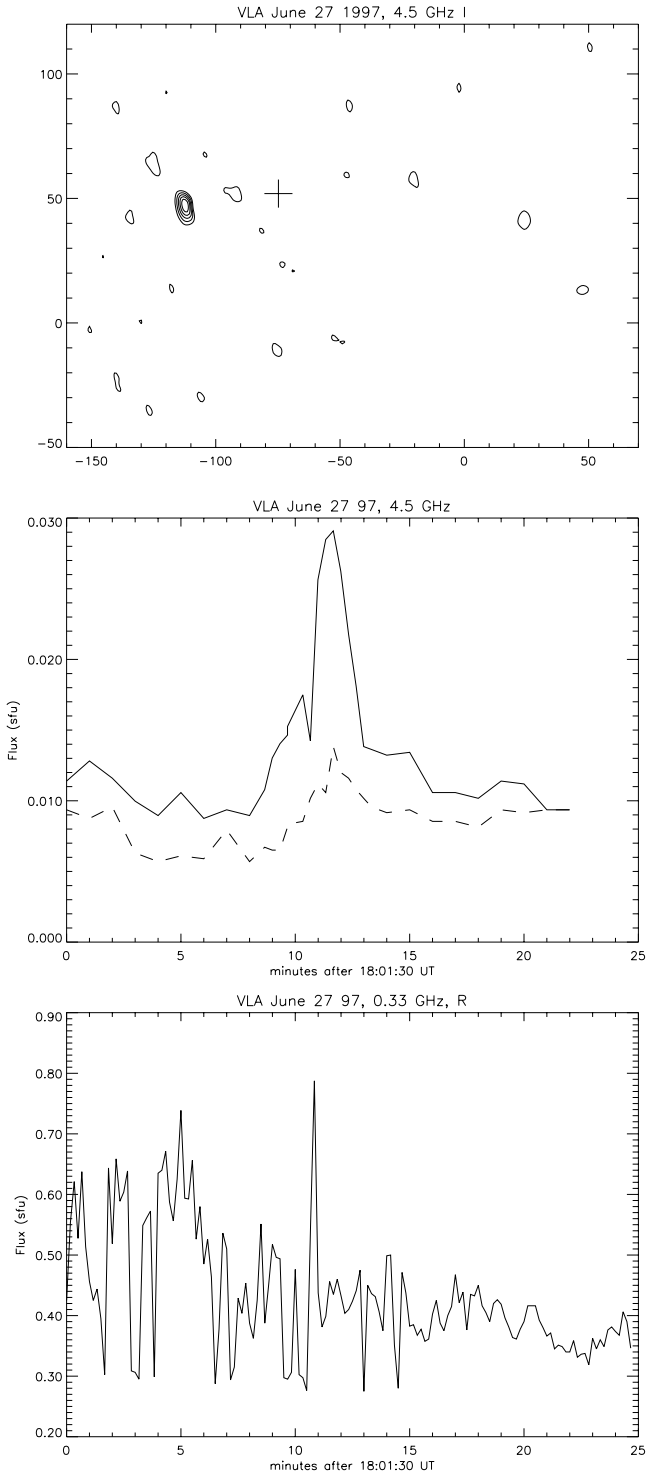

FIG. 3.—June 27 18:13 UT TB. Snapshot 4.53 GHz image of the TB at the time of its maximum (*top frame*). The contours are at multiples of −3, 3, 4, 5, 6, 7, 8, 9, and 10 of 35,000 K. Time profiles of the radio emission from the TB at C band (*middle frame*) and P band (*bottom frame*). In the radio time profiles, full lines indicate *R* emission, while dashed lines indicate *L* emission.

assumed that only flux variations of the snapshot *R* and *L* maps above 3 σ were significant, and we found that the uncertainties in the degrees of circular polarization were between 7% and 11%. Such a high degree of polarization is unlikely to come from the thermal free-free emission. Indeed, in order to reproduce a 35% degree of circular polarization at 4.53 GHz, an average field of 300 G is needed, which is too high for the observed values of the photospheric field. The MDI data suggested that the strongest line-of-sight photospheric magnetic field associated with the five TBs we observed was only 300 G (for the June 27 events; for the other events it was even lower). The above arguments clearly ruled out the free-free process as a possible emission mechanism for the observed TBs.

The low values of the photospheric magnetic fields associated with the TBs also ruled out the gyroresonance emission mechanism for most of the observed TBs. The third harmonic of the gyrofrequency requires a field strength of 600 G in the low corona at 6 cm, whereas the maximum line-of-sight field strength of the entire active region during our observations was about 400 G. The active region was close to the limb, and if the field was radial, the maximum photospheric field strength could only have been as high as 600 G on June 27 (heliocentric angle of 50°). In any case, the TBs occurred well away from the region of maximum field.

Finally, we consider nonthermal gyrosynchrotron emission from mildly relativistic electrons as a possible mechanism for the TBs at 4.53 GHz. Both June 27 events were observed in two frequencies, so the corresponding radio fluxes could be used for a rough estimate of the spectral index δ of the nonthermal electrons. However, such a calculation is valid only when the 0.33 GHz excess emission comes from the same electrons as the excess emission in higher frequencies. If their origin is common, then their time profiles should exhibit the same behavior. But in our cases, the P-band spike emission associated with the 18:13 UT event was clearly more impulsive than the microwave event (see Fig. 3), whereas no definite conclusions can be reached for the 14:31 UT event (Fig. 2). The June 29 and June 30 TBs were detected at 4.53 GHz only. The rms noise of the corresponding 1.46 GHz scans after the application of the method described in § 2 was about 0.03–0.04 SFU. Assuming that only flux variations above 5 σ were significant, we found an upper limit at 1.46 GHz of about 0.15–0.2 SFU. If the TBs have a nonthermal optically thin spectrum with $\delta = 3$, then the 1.46 GHz fluxes extrapolated from the 4.53 GHz measurements would be of order 0.07 SFU, i.e., below our detection limit. Therefore, we cannot determine whether these events have a spectrum that continues to increase at low frequencies or whether (like flares) they are optically thick at 1.46 GHz with a turnover frequency in the microwave range. In our further computations, we used $\delta = 3$ for all TBs.

Subsequently, we used the value of δ and the observed degree of circular polarization of the impulsive components to estimate the strength and direction of the magnetic field (see Dulk 1985). Since our target was close to the limb, we used relatively high angles between the magnetic field and the line of sight (55°–65°). Coronal magnetic fields between 50 and 100 G satisfactorily reproduced the observed degrees of circular polarization. These values of the magnetic field correspond to harmonic numbers of the gyrofrequency between 15 and 30 for the 4.53 GHz emission. It is important to note that the 100 G value was derived for the June 27 TB at 18:13 UT, which was associated with a photospheric field of 300 G. The 50 G values were derived for the June 30 event and the June 29 19:03 UT events. In both cases the photospheric field was not really measurable.

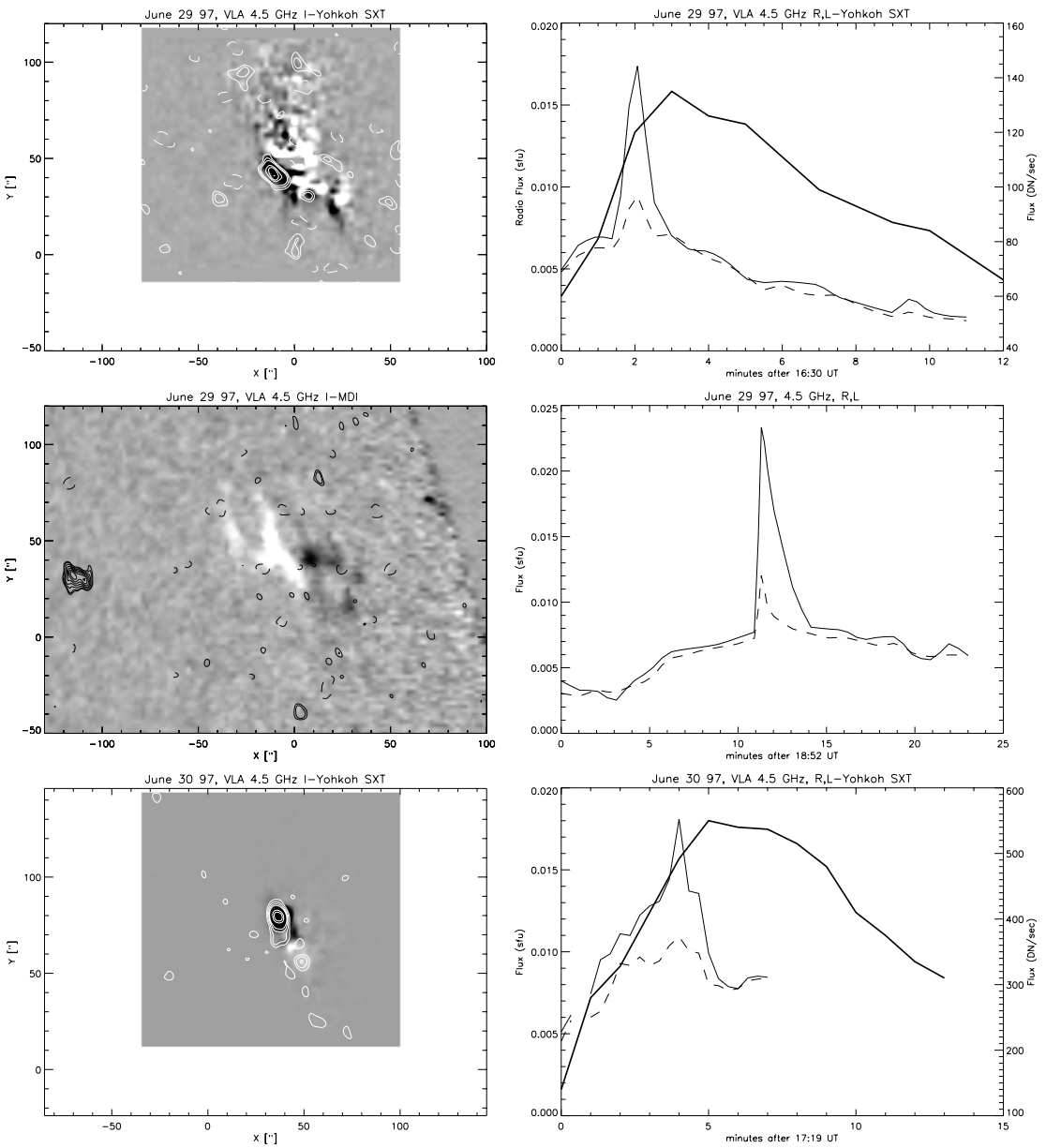

FIG. 4.—June 29 and June 30 TBs. Each row represents one TB (*top row*: the June 29, 16:32 UT TB; *middle row*: the June 29, 19:03 UT TB; *bottom row*: the June 30 TB). Top left-hand panel: Snapshot VLA 4.53 GHz image of the TB at the time of maximum, overlain on a *Yohkoh* difference image (negative display) corresponding to the time of the SXT maximum of the TB and the June 29 SXT image presented in Fig. 1. The radio contours are at multiples of –2, 2, 3, 4, 5, 8, 9, and 10 of 14,000 K. Top right-hand panel: Time profile of the TB microwave emission in *R* and *L* together with the associated soft X-ray time profile (*thick line*). Middle left: snapshot VLA 4.53 GHz image of the TB at the time of maximum, overlain on a MDI longitudinal magnetogram obtained at 20:48 UT. The radio contours are at multiples of –3, 3, 4, 5, 6, 7, 8, 9, and 10 of 13,000 K. No trace of steady photospheric field could be measured at the location where the TB occurred. Middle right-hand panel: Time profile of the TB microwave emission in *R* and *L*. Bottom (*left and right panels*): Same as in the top frames of this figure for the June 30 TB. The radio contours are at multiples of –2, 2, 4, 5, 8, 9, and 10 of 15,000 K. The *Yohkoh* difference image (negative display) corresponds to the time of the SXT maximum of the TB and the June 30 SXT image presented in Fig. 1.

For the June 29 16:32 UT TB we found a coronal field of 80 G, while the maximum value of the associated photospheric field was 170 G.

The values of the magnetic field and the angle between the magnetic field and the line of sight were used to derive the quotient between the emission coefficient and the density of nonthermal electrons. Once the emission coefficient is computed, the calculation of the corresponding brightness temperature (or flux) is straightforward, provided that the coronal plasma is optically thin. The observed brightness temperatures were reproduced assuming densities of nonthermal electrons between 1.8×10^4 and 4.4×10^4 cm^{-3}. These values were only small fractions of the total number of electrons contained in the TB loops. The total number of nonthermal electrons was of order 10^{28}, implying that the total energy released during the impulsive peaks of the radio TBs was of order 10^{26} ergs, in rough agreement with the results of Gopalswamy et al. (1997).

For the case of the 1.46 GHz TB, our data set was not sufficient to make any quantitative computations. Bastian (1991) detected transient microbursts at 1.4 GHz with flux comparable to the flux of our 1.46 GHz TB. These microbursts may be the decimeter analog to the type III micro-

bursts observed at meter wavelengths (Kundu et al. 1986). In the case of our event, the P-band type III–like emission occurred before the peak of the 1.46 GHz emission, which makes it unlikely that both frequencies were produced by the same type III event. However, the impulsive rise of the radio time profile of our TB together with the spatial and temporal association with a P-band "spike" implied a nonthermal emission mechanism.

6. CONCLUSIONS

We have analyzed 3 days of VLA observations to determine the properties of radio-selected TBs. Most previous studies of TBs analyzed data sets that were mostly soft X-ray selected (e.g., White et al. 1995; Gary, Hartl, & Shimizu 1997). The TBs were detected on the VLA maps, and subsequently we tried to relate them to soft X-ray images from *Yohkoh* or EIT. Basically, our study of the radio TBs that were also observed in soft X-rays was consistent with previous radio/X-ray comparisons. The spotless active region that we observed revealed TBs of extremely weak flux (with the exception of the 1.46 GHz event) of order 0.02 SFU; thus, they were more than 1–2 orders of magnitude weaker than the TBs presented by White et al. (1995) and Gary et al. (1997). Their flux was comparable to the flux of two of the events studied by Gopalswamy et al. (1997), which were associated with the penumbra of a large sunspot. On the other hand, they were about 4 times stronger than the events described as network flares by Krucker et al. (1997). Four out of five TBs that we detected occurred at the edge of the active region, but one occurred 100″ away from the active region, at a location where no steady coronal or chromospheric/photospheric emission was found in the available data.

We conclude that the emission of the TBs was caused by a population of nonthermal, mildly relativistic, electrons. Several arguments supported this conclusion. The time profiles of the radio TBs showed impulsive peaks while the corresponding soft X-ray time profiles were more gradual. The soft X-ray peaks were delayed with respect to the radio peaks (see Neupert 1968; Gary et al. 1997). The impulsive radio peaks showed polarization of about 30%–35%, which cannot be of thermal origin since the underlying photospheric magnetic field was weak. Our calculations showed that a small population of nonthermal electrons with spectral index $\delta = 3$ reproduced satisfactorily the basic observable characteristics of the radio TBs. The density of the required nonthermal electrons was 1.8×10^4 to 4.4×10^4 cm^{-3}, which might be only a small fraction of the total number of electrons contained in the TB loops. However, these quantities must be regarded as extremely crude estimates because of the several assumptions involved.

Our study provided new information on the TBs. In a recent study, Gary et al. (1997) presented some events that showed evidence of nonthermal emission. The TBs that we detected were 1–2 orders of magnitude weaker, but their emission mechanism was also nonthermal gyrosynchrotron. This implies that a population of mildly relativistic electrons can be present not only in the stronger TBs, but also in the weakest ones, including events occurring well away from active regions. The OVRO data used by Gary et al. (1997) were not spatially resolved, thus it was impossible to derive definite conclusions about the location of the nonthermal sources or any quantitative information about the nonthermal electrons. Our work removes, to some extent, these uncertainties. It seems that nonthermal TBs can be detected anywhere on the solar disk: near large sunspots with strong magnetic fields (Gopalswamy et al. 1997), at the edge of weak active regions with practically no sunspots (present study), or even away from active regions (Krucker et al. 1997; this paper).

The selection method might also have an impact on the final results. Two striking examples that demonstrate this argument are the study by White et al. (1995) and the present study. The former detected only thermal TBs that were X-ray selected, while we detect only nonthermal TBs that were microwave selected. This is not surprising, since the origin of the soft X-ray emission is thermal, while the microwave observations could be sensitive to both thermal and nonthermal emission mechanisms. The higher frequency used by White et al. (1995) is more sensitive to thermal emission. However, we should point out that with enough sensitivity even high-frequency observations of TBs could reveal nonthermal signatures (as was the case for the observations of Krucker et al. 1997). Our data set allowed us to study interesting manifestations of TBs that have not been observed before and could not be revealed using soft X-rays observations only, i.e., the excess P-band type III–like emission associated with two TBs of our collection and the detection of a TB away from the active region at a location where no steady emission was established from the available data. Our detection of a bright nonthermal TB well away from any active region together with the observations of Krucker et al. (1997) show that acceleration of electrons to nonthermal energies can take place even in the quiet solar atmosphere.

We would like to thank N. Nitta for providing us the *Yohkoh* SXT data. This research at the University of Maryland was carried out with support from NSF grant ATM 96-12738 and NASA grant NAG 5-6257. We thank the referee, T. S. Bastian, for his comments, which led to significant improvement of the paper.

REFERENCES

Bastian, T. S. 1991, ApJ, 370, L49
Dulk, G. A. 1985, ARA&A, 23, 169
Gary, D. E., Hartl, M., & Shimizu, T. 1997, ApJ, 477, 958
Gopalswamy, N., Payne, T. E. W., Schmahl, E. J., Kundu, M. R., Lemen, J. R., Strong, K. T., Canfield, R. C., & de la Beaujardiere, J. 1994, ApJ, 437, 522
Gopalswamy, N., Zhang, J., Kundu, M. R., Schmahl, E. J., & Lemen, J. 1997, ApJ, 491, L115
Krucker, S., Benz, A. O., Bastian, T. S., & Acton, L. W. 1997, ApJ, 488, 499
Krüger, A. 1979, Introduction to Solar Radio Astronomy and Radio Physics (Dordrecht: Reidel)
Kundu, M. R., Gergely, T. E., Szabo, A., Loiacono, R., & White, S. M. 1986, ApJ, 308, 436
Neupert, W. M. 1968, ApJ, 153, L59
Shimizu, T. 1994, PASJ, 47, 251
Shimizu, T., Tsuneta, S., Acton, L. W., Lemen, J. R., Ogawara, Y., & Uchida, Y. 1994, ApJ, 422, 906
Shimizu, T., Tsuneta, S., Acton, L. W., Lemen, J. R., & Uchida, Y. 1992, PASJ, 44, L147
Tsuneta, S., et al. 1991, Sol. Phys., 136, 37
Wang, H., Zirin, H., & Ai, G. 1991, Sol. Phys, 131, 53
White, S. M., Kundu, M. R., Shimizu, T., Shibasaki, K., & Enome, S. 1995, ApJ, 450, 435